Astron. Astrophys. 292, 341–349 (1994)

ASTRONOMY AND ASTROPHYSICS

The many incarnations of accretion disk dynamos: mixed parities and chaos for large dynamo numbers

Ulf Torkelsson[1]* **and Axel Brandenburg**[2]

[1] Lund Observatory, Box 43, S-221 00 Lund, Sweden
[2] HAO/NCAR**, P.O. Box 3000, Boulder, CO 80307, USA

Received 28 February 1994 / Accepted 9 July 1994

Abstract. We study nonlinear accretion disk dynamos, and demonstrate that different types of magnetic field configurations will arise depending on the dynamo number. Dynamo action is parametrised by the α-effect, whose strength is determined by a dimensionless number C_α. Using α-quenching as the only nonlinearity, we find for $C_\alpha > 0$ that a steady quadrupolar field is first excited. However this solution disappears before any other field configuration is excited. Thus there is a gap without any magnetic field. This is a feature of the particular nonlinearity used, and has not been observed previously in other systems. At higher dynamo numbers oscillatory dipolar and quadrupolar fields emerge, and later the quadrupolar solution bifurcates to a chaotically varying mixed parity solution. Finally, at extremely high dynamo numbers the chaotic field transforms into a steady mixed parity solution, which is dominated by an even parity component. For $C_\alpha < 0$ we first find an oscillatory dipolar field, which bifurcates to a doubly periodic mixed parity field, and later also to a chaotically varying field. Using magnetic buoyancy as the nonlinearity the gap no longer occurs. However we are not able to go to as high dynamo numbers as before. Nevertheless for the entire interval investigated, we only find a steady quadrupolar field for $C_\alpha > 0$, and an oscillatory quadrupolar or dipolar field for $C_\alpha < 0$.

Key words: accretion: accretion disks – magnetic fields – MHD – chaotic phenomena – novae, cataclysmic variables

1. Introduction

In a previous paper (Torkelsson & Brandenburg 1994a, hereafter Paper I), we have presented linear models of accretion disk dynamos, and also a few examples of nonlinear dynamos. However when comparing the critical dynamo numbers of Paper I with estimates of the dynamo numbers in real accretion disks, the predictions of linear theory become irrelevant, because the estimated dynamo numbers for accretion disks are orders of magnitude larger than the critical ones. Thus there is a need for a systematic survey of nonlinear accretion disk dynamos.

The geometry of the disks considered here is obviously too thick to be directly applicable to real accretion disks. Nevertheless, many of the bifurcation patterns we find here appear to be typical for Keplerian disks. Moreover, there is a variety of new features of solutions in the highly nonlinear regime that have not been found previously in other geometries. In this sense we consider the present investigation as an important step towards understanding nonlinear dynamos in flat geometries.

The nonlinearities in the dynamo are typically caused by the action of the magnetic field on the motion of the plasma. An example is α-quenching, by which the magnetic field modifies the small scale turbulence and diminishes the α-effect that generates a large scale magnetic field from the small scale fluctuations. Another nonlinear effect, which may also be important for accretion disks, is magnetic buoyancy. It leads to a vertical transport of magnetic field out of the disk, because the magnetic pressure inside a magnetised region decreases its density.

A partial survey of nonlinear solutions was presented by Torkelsson & Brandenburg (1994b, hereafter Paper II). The main aim was to investigate the route to chaos for an α-effect that is negative above the disk midplane and positive below (i.e. $C_\alpha < 0$). The present paper, on the other hand, aims at presenting a more complete investigation of the different manifestations of accretion disk dynamos over a larger part of the parameter regime, both for positive and negative values of the α-effect.

A summary of the mathematical formulation is given in Sect. 2. The results for α-quenching are given in Sect. 3. Section 4 contains the corresponding results for magnetic buoyancy. Section 5 investigates the importance of the spatial variation of the nonlinearities. A general discussion of the results are given in Sect. 6, and finally Sect. 7 contains the conclusions.

Send offprint requests to: Ulf Torkelsson, (Utrecht address)
* Present address: Sterrenkundig Instituut, Postbus 80000, NL-3508 TA Utrecht, The Netherlands
** The National Center for Atmospheric Research is sponsored by the National Science Foundation

2. Formulation of the problem

The evolution of the mean-field dynamo is described by

$$\frac{\partial \boldsymbol{B}}{\partial t} = \boldsymbol{\nabla} \times (\boldsymbol{u} \times \boldsymbol{B} + \alpha \boldsymbol{B} - \eta_t \mu_0 \boldsymbol{J}), \quad \boldsymbol{\nabla} \cdot \boldsymbol{B} = 0, \tag{1}$$

where $\boldsymbol{B}$ is the mean magnetic field, $\boldsymbol{J} = \boldsymbol{\nabla} \times \boldsymbol{B}/\mu_0$ the mean current density, $\boldsymbol{u}$ the mean velocity, α describes the α-effect, η_t the turbulent magnetic diffusivity, and μ_0 the magnetic permeability of free space. We solve Eq. (1) in spherical polar coordinates (r, θ, ϕ) using the same method, units, and boundary conditions as in Paper I. Length, time and velocity are measured in units of

$$[r] = R, \ [t] = R^2/\eta_{\rm disk}(R), \ [u] = \eta_{\rm disk}(R)/R, \tag{2}$$

where R is the outer radius of the computational grid, and $\eta_{\rm disk}$ the turbulent magnetic diffusivity in the disk. The strengths of differential rotation and α-effect are quantified, respectively, by the dynamo numbers

$$C_\alpha = \frac{\alpha_0 R}{\eta_{\rm disk}(R)}, \ C_\Omega = \frac{\Omega_0 R^2}{\eta_{\rm disk}(R)}, \tag{3}$$

where Ω_0 is the angular velocity at some reference distance ϖ_0.

We assume a disk with an inner radius $\varpi_0 = 0.15$ and an outer radius $R = 1$, i.e. coincident with the outer boundary of the grid, and a constant vertical half-thickness $z_0 = 0.2$. The disk has a Keplerian rotation law with Ω independent of z. Outside the disk we put $\Omega = 0$. We also neglect the effect of the radial inflow, as it is slower than both the rotation and the turbulent motions. Inside the disk the diffusivity $\eta_{\rm disk} \propto \varpi^{1/2}$, where ϖ is the distance from the rotational axis, with the normalisation $\eta_{\rm disk} = 0.1$ at $\varpi = 1$, whereas the diffusivity is unity outside the disk.

Our disk model is unrealistically thick, and it also lacks the flaring shape characteristic of true accretion disks. However, it was found in Paper I that the dynamo is insensitive to the exact shape of the disk, and that even a disk as thick as ours yields solutions typical for thinner disks. A much thinner disk model would be more demanding in terms of computer resources. Thus, for the purpose of a qualitative investigation covering a broad parameter space we chose a thick disk model as a reasonable compromise. Another problem is the limited difference in magnetic diffusivities between the accretion disk and the surrounding pseudo-vacuum, but from tests in Paper I, we do not believe that this is a serious problem, especially since we shut off the differential rotation outside the disk.

According to mean-field dynamo theory, α exists only in the presence of a vertical gradient in the density ρ and/or the turbulent intensity u_t, with $\alpha \sim -\Omega H^2 \frac{d}{dz} \ln(\rho u_t)$ (Krause 1967, Rüdiger & Kitchatinov 1993), where H is the disk height. If the stratification in ρ is dominant, one gets for isothermal disks $\rho = \rho_0 \exp(-z^2/H^2)$ and $\alpha \sim +z\Omega$. In the context of the solar dynamo it turned out that the solar magnetic field geometry can be explained if α is formally governed by the gradient of u_t alone (Rüdiger & Brandenburg 1994). It is therefore tempting to consider such a case also. Assuming ρu_t^2=const, we would have $\alpha \sim -z\Omega$. We take for the α-effect with α-quenching the expression

$$\alpha = \alpha_0 z \frac{\Omega}{\Omega(\varpi_0)} \frac{1}{1 + \alpha_B \boldsymbol{B}^2} \tag{4}$$

inside the disk and $\alpha = 0$ outside, where α_0 can have both signs. Here, α_B is a measure of the nonlinearity. We expect $\alpha_B = 1/\boldsymbol{B}_{\rm eq}{}^2$, where $\boldsymbol{B}_{\rm eq}$ is the field strength corresponding to equipartition between the magnetic field and the turbulent velocity. Nonlinear dependencies of α on $\boldsymbol{B}$ have frequently been studied in dynamo theory (e.g. Stix 1972). The linear part of this expression is similar to that used by Stepinski & Levy (1991), which was derived from an analogy with stellar dynamos. A more reliable derivation is desirable, but not possible for the moment as there is no detailed theory for the turbulence in disks. By setting $\alpha_B = 1$ we define a unit for the magnetic field, i.e. $[B] = B_{\rm eq}$. This is different from the definition in Paper I, but physically more palatable.

For a dynamo with magnetic buoyancy, but no α-quenching, we set $\alpha_B = 0$ and introduce an additional velocity field

$$\boldsymbol{u}_B = \gamma_B \boldsymbol{B}^2 \boldsymbol{z}, \tag{5}$$

where γ_B describes the strength of the buoyancy (see Eq. (17) in Paper I, where $\hat{\boldsymbol{z}}$ should read $\boldsymbol{z}$). Again it is convenient to put $\gamma_B = 1$, which yields a unit for the magnetic field. In general it is expected that α_B and γ_B are functions of ϖ. However it was found in Paper I that this does not qualitatively change the character of the dynamo, and the results in Sect. 5 confirm this. Thus, for simplicity we use constant values for α_B and γ_B.

It is of interest to discuss the parity of the generated field, not only from a dynamo theoretical point of view, but also to address the question to what extent the magnetic field is able to accelerate a jet from the accretion disk (e.g. Wang et al. 1992). In general the field is not of pure parity, but to estimate how close to even or odd parity the field is, we define a continuous measure of parity

$$P = \frac{E^{(\rm S)} - E^{(\rm A)}}{E^{(\rm S)} + E^{(\rm A)}}, \tag{6}$$

where $E^{(\rm S)}$ and $E^{(\rm A)}$ are the energies of the symmetric and antisymmetric parts of the magnetic field, respectively.

3. Results for a dynamo with α-quenching

A partial investigation of the nonlinear disk dynamo with α-quenching was presented in Paper II. Here we continue and extend this investigation. All our simulations are carried out on 41×41 or 41×81 uniformly spaced grid points in the (r, θ)-plane, depending on whether we solve the equations on one quadrant, prescribing the parity of the field, or on two quadrants without imposing a specific parity on the field. We use a time step of $2.5\,10^{-6}$ in units of the magnetic diffusion time, and put $C_\Omega = 250\,000$. C_α will be in the range from the critical values determined in Paper I up to what is expected from the

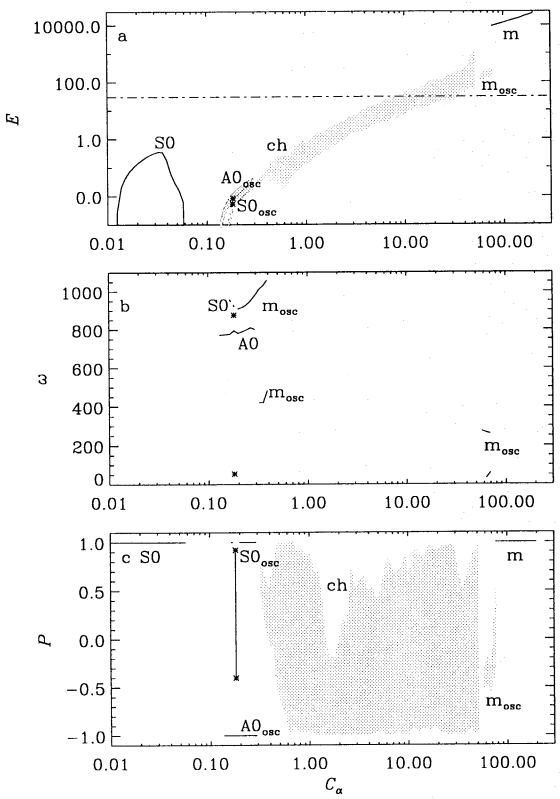

Fig. 1. a Bifurcation diagram for a disk dynamo with α-quenching, $C_\alpha > 0$, and $C_\Omega = 250\,000$. For the oscillatory and chaotically varying dynamos we have plotted the intervals within which the energy varies. The asterisks show the interval for a biperiodic solution at $C_\alpha = 0.18$ oscillatory in both E and P. S0 and A0 stand for solutions of positive and negative parity, respectively, while m and ch denote a dynamo of mixed parity and a chaotically varying dynamo, respectively. Subscript osc indicates an oscillatory solution, and dashed lines represent unstable solutions. The dash-dotted line indicates equipartition between magnetic pressure and gas pressure. **b** The frequencies of the regularly oscillating dynamos. The asterisks mark the two frequencies of the biperiodic solution. **c** The parity of the saturated fields as a function of C_α. The asterisks mark the interval, within which the biperiodic solution is oscillatory

simple order of magnitude estimates in Paper I. These numbers are up to four orders of magnitude above the critical dynamo numbers, because the strong differential rotation makes it possible to excite the dynamo already at very small values of C_α. As a matter of fact, C_α is still much smaller than C_Ω at these values, that is the turbulent velocities are still much smaller than the rotational velocities in accordance to the assumptions of thin accretion disk theory. The calculations were repeated for a thinner disk, $z_0 = 0.15$, with the same qualitative results.

Below we will treat the cases with a positive and a negative α-effect separately. In the following we denote pure quadrupolar and dipolar solutions as S0 and A0, respectively. For further details we refer to Paper I.

3.1. $C_\alpha > 0$

A bifurcation diagram for $C_\alpha > 0$ is shown in Fig. 1a. There first appears a steady S0 solution at $C_\alpha = 0.012$, which is predicted by linear theory (Stepinski & Levy 1988). However, this solution dies out at $C_\alpha = 0.063$, before any other solution is excited. This is in partial agreement with the calculations of the linear growth rates by Stepinski & Levy (1991), as they find that the linear growth rate becomes negative for large values of C_α. Later there appear oscillatory A0- and S0-solutions at $C_\alpha = 0.14$ and 0.16, respectively, but initially the quadrupolar solution is unstable, and evolves to the dipolar. The angular frequencies, ω, of these solutions are shown in Fig 1b. A significant difference from Stepinski & Levy (1991) is that in their Fig. 1 the oscillatory S0-solution appears before the A0-solution, and also before the steady S0-solution has disappeared, but the parameters of their model differ somewhat from ours.

The frequencies of the two solutions approach each other, until there appears a biperiodic, mixed parity solution oscillatory in both the magnetic energy, E, and the parity measure, P, at $C_\alpha = 0.18$ (Fig. 1c). When calculating the power spectrum of the variations in magnetic energy for the biperiodic solution, three peaks actually appear, but the weakest coincides with the beat frequency of the other two, and the strongest is that found already for the S0-solution. Beyond this point both the S0- and A0-solutions are stable, and an arbitrary initial state will evolve to either one of them, depending on the initial parity. The solutions of fixed parity later become unstable, and instead a solution oscillatory in both the magnetic energy and parity measure appears. It is evident from Figs. 1a and c that this mixed parity solution bifurcates from the S0-solution. At $C_\alpha = 0.43$ it has become chaotic. Figure 1c demonstrates that even if the mixed parity solution originates from the even parity solution, after increasing C_α by only a factor of two, the field can attain configurations of any parity.

As the mixed parity solution becomes chaotic, the peaks in the power spectrum first broaden, and for increasing values of C_α, the continuum starts to dominate. A few humps may still be present at much higher values of C_α, albeit they contain only a minor part of the power. As an example we show the time series of the magnetic energy, and the corresponding power spectrum for a model with $C_\alpha = 0.69$ in Fig. 2. The largest Lyapunov exponent for this solution is approximately 17. The fact that it is positive demonstrates that it is truly chaotic. The Lyapunov exponent is comparable to the inverse of the diffusion time scale and of the same order of magnitude as was found for chaotic solutions with $C_\alpha < 0$, see Paper II.

At $C_\alpha = 57.2$, the dynamo again becomes oscillatory and of mixed parity, but the oscillations are non-sinusoidal. The oscillations have become biperiodic at $C_\alpha = 63$ with the frequencies $\omega = 262$ and 31.3. Later the solution undergoes a new bifurcation to a steady solution of much higher energy. The steady solution has P close to 1, but the parity measure appears to continue evolving slowly even after the energy has settled onto a definite value. As there appears a steady solution with a well-ordered magnetic field at extremely supercritical dynamo numbers we

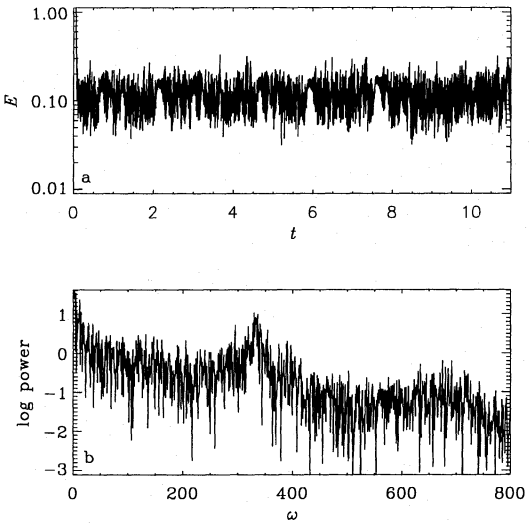

Fig. 2. a The evolution of the magnetic energy for a model with α-quenching and $C_\alpha = 0.69$. **b** Power spectrum of magnetic energy

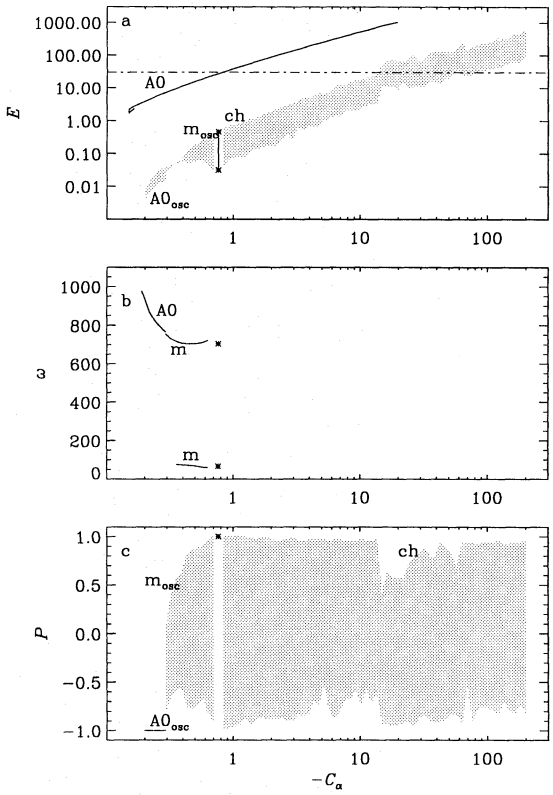

Fig. 3. a Bifurcation diagram for a disk dynamo with α-quenching, $C_\alpha < 0$, and $C_\Omega = 250\,000$. The symbols have the same meanings as in Fig. 1. The asterisks show the interval for a biperiodic solution at $C_\alpha = -0.76$ oscillatory only in E. **b** The frequencies of the regularly oscillating dynamos. The asterisks mark the two frequencies of the biperiodic solution. Note that the mixed parity solution has become triply periodic at $C_\alpha = -0.63$, but the third frequency $\omega = 15$ has not been included in the figure. **c** The parity of the saturated fields as a function of C_α. The asterisk marks the even parity of the biperiodic solution

are confident that the resolution is sufficient to yield reliable solutions even for highly supercritical dynamo numbers. Since the estimates and preliminary investigations in Paper I indicated that accretion disks should not exist at higher dynamo numbers than the ones leading to this type of solution, we have not continued the search at higher dynamo numbers.

3.2. $C_\alpha < 0$

Figure 3a shows the bifurcation diagram for negative C_α. The main feature in the diagram is the transition from an oscillatory A0-solution via a mainly biperiodic mixed parity solution to a chaotic one at sufficiently high dynamo numbers, which was discussed at length in Paper II. The frequencies and parity measures of the oscillatory A0 and mixed parity solutions are plotted in Figs. 3b and c, respectively. There are simultaneous jumps in E and P at $C_\alpha = -14.9$. After this discontinuity there are no longer any distinguishable humps in the power spectrum of the energy fluctuations. Note that the unstable oscillatory S0-solution is not included in the diagram because it overlaps with the oscillatory A0 and mixed parity solutions.

The origin of the steady A0-solution in the upper left corner of Fig. 3a is somewhat obscure, especially because we have not been able to follow it to smaller magnetic energies, and it only appears for a sufficiently strong seed field, thus we expect it to emerge from a subcritical bifurcation. At $C_\alpha = -19.8$ it starts to show signs of rapid oscillations of very low amplitude. At this point it becomes unstable and evolves toward the chaotic mixed parity solution, provided it is not constrained to be of odd parity.

4. Results for a dynamo with magnetic buoyancy

Test calculations with magnetic buoyancy showed that the same spatial resolution was sufficient, but that a smaller time step of 10^{-6} was needed.

4.1. $C_\alpha > 0$

The bifurcation diagram for the case with magnetic buoyancy and positive C_α is plotted in Fig. 4. An important difference to the case with α-quenching is that the previous gap with no magnetic field generation has disappeared. Apart from the steady S0-solution, the only other solution found is unstable and of A0 type. By restricting ourselves to odd parity only, we found indications that this solution emerges via a subcritical bifurcation, because it appears already before the linear growth rate becomes positive around $C_\alpha = 0.1$. Comparing to Fig. 1 one would expect to find an oscillatory S0-solution close to the A0-solution in Fig. 4a. Although we have not found it, it is still possible that it exists as an unstable oscillatory S0-solution. Due to numerical

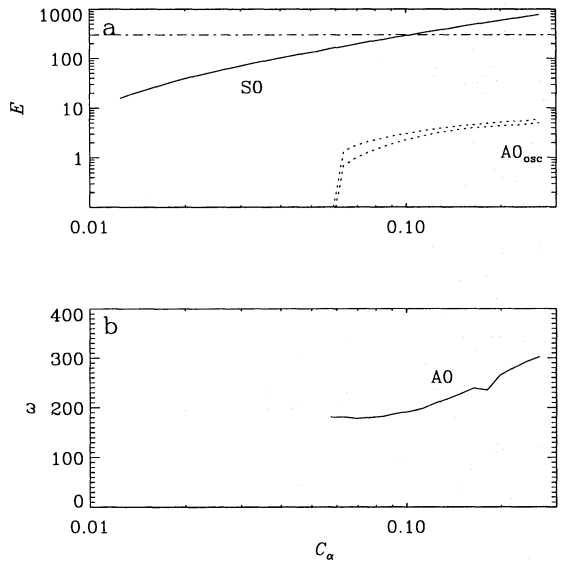

Fig. 4. a The bifurcation diagram for a disk dynamo with magnetic buoyancy, $C_\alpha > 0$, and $C_\Omega = 250\,000$. The symbols have the same meanings as in Fig. 1. **b** The frequencies of the regularly oscillatory dynamos

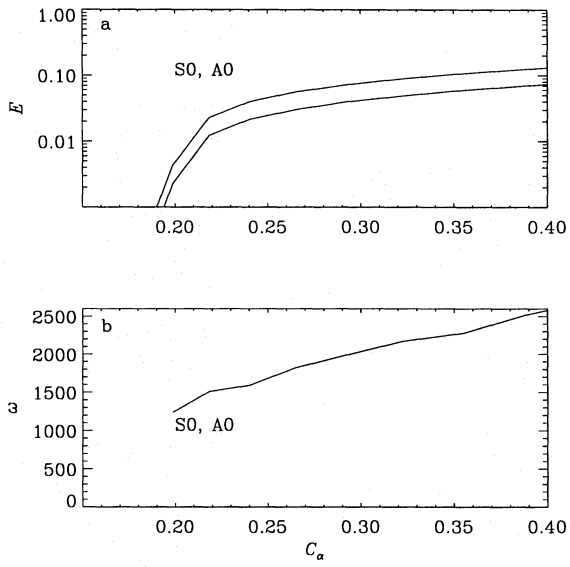

Fig. 5. a Bifurcation diagram for a disk dynamo with magnetic buoyancy, $C_\alpha < 0$, and $C_\Omega = 250\,000$. The symbols have the same meanings as in Fig. 1, but note that now the abscissa is linear. **b** The frequencies of the regularly oscillatory dynamos

stability problems we were unable to continue these calculations to as high dynamo numbers as for α-quenching.

4.2. $C_\alpha < 0$

The bifurcation diagram for this case is shown in Fig 5. As found already in Paper I, there are oscillatory S0- and A0-solutions, both of which are stable for most of the interval investigated. They have also similar energies and frequencies. The reason for this can be understood by looking at Fig. 13 in Paper I, showing that dynamo action takes place in two distinct belts close to the upper and lower surface of the disk. Consequently, both toroidal and poloidal fields are vanishing at the midplane of the disk. Thus, the fields above and below the midplane are decoupled. Since the induction equation is invariant under change of sign of $\boldsymbol{B}$, even and odd parity solutions are possible that only differ in the direction of $\boldsymbol{B}$ in one of the two hemispheres. Apart from that, the field geometries are the same.

5. Towards more realistic models

In this section we address some aspects that need to be taken into account when more realistic and consistent models are to be constructed. Several issues, including the necessity to consider thinner disk geometries, have already been discussed in Paper I. Here we focus on more consistent profiles for the various coefficients.

5.1. Spatial dependence of α_B and γ_B

As was discussed in Paper I, a more realistic description of the nonlinear effects should include the spatial dependence of α_B and γ_B. We have recalculated a number of models using the same spatial dependencies as in Paper I to see whether they cause any significant deviations. We assume $\alpha_B \propto \varpi^3$ and $\gamma_B \propto \varpi^2$ (Paper I) and normalise so that the parameters keep their old values at $\varpi = 1$. These profiles mean essentially that the disk is able to host a stronger field in its innermost region.

Several trial computations showed that the basic types of stable solutions remain unchanged for spatially dependent profiles of α_B and γ_B, except that the total magnetic energies increase as the α-quenching or buoyancy become weaker in the inner parts of the disk. We compare the poloidal fields of the steady solutions for $C_\alpha = 0.0325$ with $\alpha_B = 1$ and $\alpha_B = \varpi^3$ in Fig. 6. In Fig. 7 we also show for the two models the root-mean-square of the poloidal fields at the surface of the disk, and the rms-value over cylinders for the toroidal fields. This picture shows quite clearly the strong similarity between cases with and without spatially varying α_Bs.

5.2. The vertical stratification and consistency of profiles

Traditionally, dynamo theory asks the question whether a magnetic field can be generated from a given velocity field. This velocity field, which consists of both the large scale (Keplerian) motion and the small scale turbulent motions, must be a

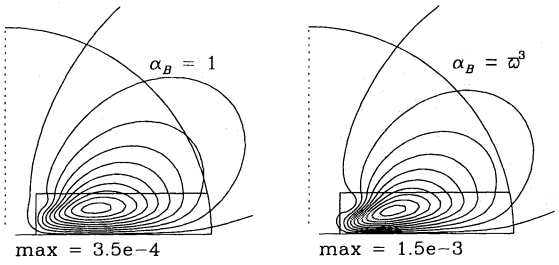

Fig. 6. The poloidal fields of nonlinear dynamos with α-quenching, $C_\Omega = 250\,000$, and $C_\alpha = 0.0325$. To the left for $\alpha_B = 1$, and to the right for $\alpha_B = \varpi^3$

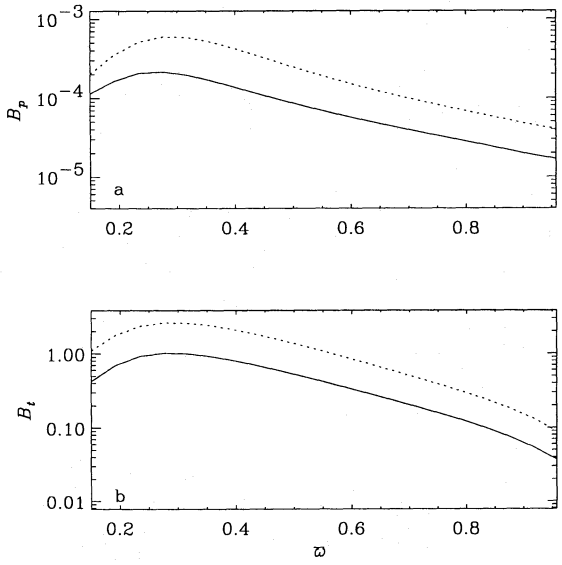

Fig. 7. a The poloidal rms-field at the surface of the accretion disk for a nonlinear dynamo with α-quenching, $C_\Omega = 250\,000$, and $C_\alpha = 0.0325$. The solid lines represent a model with $\alpha_B = 1$, and the dashed lines a model with $\alpha_B = \varpi^3$. **b** The rms-value of the toroidal field taken over cylinders across the disk

solution of the equations of motion. The turbulent velocity field contributes to the vertical pressure equilibrium via the equation

$$\frac{d}{dz}\left(\tfrac{1}{3}\rho u_t^2 + p_{\rm gas}\right) = -\rho\Omega^2 z, \tag{7}$$

where $p_{\rm gas}$ is the gas pressure and the density ρ enters in the profile for $\alpha \propto -\frac{d}{dz}\ln(\rho u_t)$; see the introduction. This approach has recently been persued by Rüdiger et al. (1994) in an attempt to construct a consistent dynamo model of a standard accretion disk.

In our models we used a constant profile for η_t in the vertical direction. With $\eta_t = \frac{1}{3}u_t^2\tau_{\rm corr}$, and a constant correlation time $\tau_{\rm corr}$, this corresponds to a constant profile of u_t. Assuming for simplicity an isothermal disk, i.e. $p_{\rm gas}/\rho = c_s^2$ =const, this leads to

$$\alpha \propto -\Omega H^2 \frac{d\ln\rho}{dz} = \Omega z(1 + \tfrac{1}{3}{\rm Ma}^2)^{-1} \tag{8}$$

i.e. there is no deviation from the $\alpha \propto z$ profile, that was assumed in the present investigation. In this sense the profiles used in our models with $C_\alpha > 0$ are indeed consistent. $C_\alpha < 0$ can arise from a density inversion, as has been found by Milsom et al. (1994), or if we only consider the velocity stratification while calculating α. The later approach can be made consistent with the disk model if it is assumed that $\tau_{\rm corr}$ is a decreasing function of $|z|$, and that the turbulence is always subsonic, so that it does not affect Eq. 7. There is no theoretical justification for neglecting the density stratification, however Rüdiger & Brandenburg (1994) found it possible to reproduce the solar magnetic field by assuming that the α-effect arises formally only from the velocity stratification.

5.3. The nature and spatial variation of the turbulence

The most severe obstacle in modelling accretion disks in general, and accretion disk dynamos in particular, are our lack of knowledge of the disk turbulence. The gravest problem is connected to the vertical variation of the turbulence, which determines the sign of C_α. As the standard model by Shakura & Sunyaev (1973) uses vertically averaged quantities, it does not provide any information on the vertical distribution of the turbulence, and actually its viscosity description is merely a parameterisation of our lack of knowledge of the nature of the turbulence. Several authors have attempted to derive the Shakura-Sunyaev parameter $\alpha_{\rm SS}$ from first principles (e.g. Meyer & Meyer-Hofmeister 1982, Eardley & Lightman 1975, Vishniac & Diamond 1989), but there is no agreement on the relevant physics. For this reason we have considered it sufficient to use α- and η_t-profiles that reproduce a few properties that are likely to be found also in a realistic turbulence model.

6. Discussion

6.1. Bifurcation behaviour of the nonlinear dynamo

We concentrate here mainly on cases with $C_\alpha > 0$, because those with $C_\alpha < 0$ were already discussed in Paper II. The first interesting property is the gap between the steady S0-solution and the oscillatory A0-solution. At first one may think of this being a consequence of the linear growth rate becoming negative. However, we know of at least two counterexamples demonstrating that this is not sufficient. Firstly we find that with magnetic buoyancy instead of α-quenching the S0-solution continues through the magnetic gap. Brooke & Moss (1994) find that for dynamos in torus geometry with Keplerian rotation the linear growth rate of the S0-solution becomes negative at a sufficiently high dynamo number. However, when they start the nonlinear calculation from a strong seed field they still find a non-trivial solution (Brooke, private communication). We also find that for our α-quenched dynamo the linear growth rate becomes negative before the nonlinear solution disappears. This shows that there are cases beyond the first bifurcation, where a positive linear growth rate is not even a necessary condition for dynamo action. Furthermore, this result indicates that the difference to the model of Brooke & Moss is mainly quantitative: in both

cases α-quenching tries to bridge the gap, but it is only partially successful in our case.

Another interesting question regards the stability of the oscillatory A0-solution. With α-quenching this solution is stable, but with magnetic buoyancy it is unstable. These results are in agreement with the findings of Krause & Meinel (1988) that for a weakly nonlinear α^2-dynamo the only initially stable solution is the one bifurcating from a stable trivial solution. In our case with α-quenching the trivial solution once again becomes stable in the gap between the disappearance of the steady S0-solution and the appearance of the oscillatory A0-solution, which thus is initially stable. Later in the nonlinear regime the oscillatory S0-solution also becomes stable, and the mixed parity solution bifurcates from this one, while the oscillatory A0-solution finally becomes unstable. In the case with magnetic buoyancy there is no gap with a stable trivial solution, and therefore the oscillatory A0-solution must be (at least initially) unstable.

6.2. *Magnetic field strengths in real accretion disks*

In order to simplify the discussion we will mainly consider the accretion disk of a cataclysmic variable. What basically determines the importance of the magnetic field is its strength. In this paper we have defined the unit of the magnetic field strength by putting the parameter describing the nonlinearity to unity. As we investigate two different types of instabilities, we have to consider separately the corresponding units for the field strength. For the α-quenching case this is determined by setting the kinetic energy density of the turbulent motions equal to the energy density of the magnetic field. This gives $[B] = \sqrt{\mu_0 \rho} u_t$, where ρ is a typical density and u_t a typical value for the turbulent velocity. The typical values of these quantities are uncertain and vary widely from system to system. As an example we take a white dwarf of $M = 1 M_\odot$ accreting at a rate of 10^{13} kg s^{-1} and perform the calculations at $R = 10^7$ m. The turbulent velocity is basically unknown, but we assume that it is 10% of the sound speed, which we calculate from the hydrostatic equilibrium in the vertical direction $c_s = (H/R)(GM/R)^{1/2}$. Thus, we get $[B]_\alpha = 0.3$ T, assuming that the viscosity parameter from Shakura & Sunyaev (1973) is $\alpha_{SS} = 0.1$.

For the magnetic buoyancy case, we can start from Eq. (18) in Paper I, and after some algebraic manipulations involving standard relations for thin disks and putting the magnetic diffusivity equal to the shear viscosity as given by Shakura & Sunyaev, $\eta_{disk} = \alpha_{SS} H c_s$, we get

$$[B]_\gamma = 2 \left(\alpha_{SS} \frac{H}{R} \frac{1}{k \mathrm{Ma}^3} \right)^{1/2} [B]_\alpha. \tag{9}$$

Here, $k \approx 0.5$ is a numerical constant defined in Paper I, and Ma$= u_t/c_s$ is the Mach number of the turbulent velocity, which roughly yields $[B]_\gamma = 3[B]_\alpha \approx 1$ T (but note that these parameters are strongly dependent upon what values one chooses).

There are two important limits for the magnetic field. First of all, if the magnetic field exceeds the gas pressure (or the radiation pressure in the case of a radiation dominated disk), it will be necessary to take into account the effect of the magnetic pressure on the vertical hydrostatic equilibrium. However the thin disk approach in a general sense may still be valid, even though a consistent treatment requires the simultaneous solution of both the dynamo and the disk structure.

The second limit occurs when the disk is no longer geometrically thin or when the angular velocity deviates strongly from Keplerian rotation. The hydrostatic equilibrium in the vertical direction including the effect of magnetic pressure can then be formulated as

$$\frac{d}{dz} \left(\tfrac{1}{3} \rho u_t^2 + p_{gas} + \frac{\boldsymbol{B}^2}{2\mu_0} \right) = -\rho \Omega^2 z. \tag{10}$$

When $p_{gas} \ll \boldsymbol{B}^2/(2\mu_0)$, we may write as an order of magnitude estimate

$$\frac{u_A}{u_{Kepl}} = \frac{H}{\varpi}, \tag{11}$$

where $u_{Kepl} = \Omega \varpi$ is the Keplerian velocity, and $u_A = \boldsymbol{B}/(\mu_0 \rho)^{1/2}$ the Alfvén velocity. It can be shown that an equivalent criterion guarantees that the angular velocity is close to its Keplerian value. The condition $H/\varpi \ll 1$ allows for much larger magnetic fields than the first limit as long as $c_s/u_{Kepl} \ll 1$. Such highly magnetised states might be unstable, but this is not completely obvious since, for example, the Parker instability is less efficient in the presence of rotation and shear (Cattaneo & Hughes 1988, Foglizzo & Tagger 1994). Disks with magnetic fields exceeding this second limit are geometrically thick and cannot be treated within the thin disk formalism.

As our disk models were not based upon a calculation of the disk structure, it is difficult to apply the limits discussed above to our results. In Figs. 1, 3 & 4 we have tried to indicate when the magnetic pressure on average reaches equipartition with the gas pressure. These limits, plotted as horizontal dash-dotted lines, should only be taken as order of magnitude estimates. Note also that in Fig. 5 the magnetic field never reaches this limit. It also turned out that the magnetic field never became sufficiently strong to violate $H/\varpi \ll 1$; see Eq. (11).

In several cases the magnetic pressure exceeds the gas pressure, in particular for the steady mixed parity solutions in Fig. 1. We present these solutions merely for completeness, because the transition from a chaotic solution back to a steady solution by way of an oscillatory solution is interesting for the theory of nonlinear dynamos.

6.3. *Observational implications*

One of the main motivations for introducing a dynamo in an accretion disk, apart from that the accretion disk seems to be a favourable place for dynamo action, is that the generated magnetic field can exert a torque on the accretion disk, transporting angular momentum outwards through the disk and leading to an inflow of matter. However, that such a mechanism for the transport of angular momentum exists is a requirement for an accretion disk, so we are not able to use this as evidence for

dynamo action. Instead we have to look for some other property, which distinguishes the magnetic field from other proposed mechanisms for driving accretion.

The FWHMs of spectral lines from the inner parts of an accretion disk in a cataclysmic variable are on the order of 2 000 km s^{-1} (e.g. Marsh et al. 1987), due to the rapid Keplerian rotation. Thus, even with the most optimistic estimates of the magnetic field strength, it is impossible to measure directly any Zeeman splitting. A more sensitive technique is to measure the circular polarisation within a spectral line. This technique has been used with great success for mapping the solar magnetic field (for a review see Stenflo 1989). A main difficulty in applying this technique to accretion disks is that the magnetic field is mainly toroidal and localised inside the presumably optically thick disk. As the theory of line formation in accretion disks is still in a formative stage, it is premature to say if there are any useful lines, but the prospects appear bleak.

Many investigators have used the presence of Ca H- and K-emission as indicators of magnetic activity in late-type stars. Some authors have found that the strength of the emission is proportional to the angular velocity of the star (e.g. Skumanich 1972, Noyes et al. 1984), but there are uncertainties both concerning whether the relevant stellar parameter is the angular velocity or the Rossby number, and what is the relevant measure of the emission line (e.g. Hartmann & Noyes 1987). Horne & Saar (1991) have noted a similar relationship for the emission lines from the accretion disks of cataclysmic variables, namely that in a disk the strength of the Balmer emission lines grows in proportion to the local angular velocity. It has proven difficult to reproduce this behaviour in calculations of accretion disk spectra (e.g. Marsh 1987). Thus, Horne & Saar suggest that the emission lines can be explained by magnetic activity. However this hypothesis does not yield any estimate of the magnetic field strength. As it is known that the emission line-strength is proportional to the magnetic field strength at the surface, we would expect from the observations by Horne & Saar that the surface field is proportional to $\varpi^{3/2}$, but as is evident from Fig. 7 this is not the case for our numerical simulations. However this does not necessarily contradict the hypothesis by Horne & Saar, as what we calculate here is the mean magnetic field, whilst the local fluctuating field occurs only implicitly in the model. On the Sun it is the latter which is responsible for most of the activity.

In our chaotic models the magnetic field and torque vary irregularly on time scales on the order of a hundredth of the magnetic diffusion time scale, which can be estimated to be on the order of $4\,10^4$ s (Paper I). We therefore expect to see variations on a time scale of hundreds of seconds. This is typical for flickering. Flickering is commonly believed to originate from the hot spot, where the gas stream from the secondary hits the outer rim of the accretion disk, but Bruch & Duschl (1993) argue that the amplitude of the flickering is often too large to be explained by processes in the hot spot. They suggest that it is produced in the boundary layer between the disk and the white dwarf, where more energy is available. Let us note that our dynamo is most efficient in the inner part of the disk, and that variations in the magnetic torque may lead to varying mass flow rates leading to variations in the emitted flux. Thus, flickering may be the observable signal of a chaotic accretion disk dynamo.

Collimated outflows are observed from many types of accreting objects, most notably protostellar objects and active galactic nuclei. Among the most popular models for these are a magnetically driven outflow from the accretion disk. The efficiency of the process is dependent on the topology of the magnetic field. It is most efficient for a dipole field, even though it will work also with other field topologies (Wang et al. 1992). According to our calculations a steady dipolar field is among the least likely configurations. On the other hand we also find that the highest magnetic energies are reached in field configurations close to quadrupolar, which diminishes the importance of the efficiency argument.

7. Conclusions

We have demonstrated that for an α-quenched accretion disk dynamo, the firstly excited solutions give way to chaotic solutions of mixed parity at higher dynamo numbers. For positive C_α the solution finally becomes steady and of almost quadrupolar nature. The routes to chaos however are not straightforward, but always involve a series of bifurcations. For $C_\alpha > 0$ the firstly excited S0-solution dies out before any other solution has appeared. Then there emerge two oscillatory solutions: an A0, which is stable, and a S0, which is initially unstable. Later the S0-solution also becomes stable, and it is from this one that the mixed parity solution bifurcates, while the A0-solution becomes unstable. For $C_\alpha < 0$ there also appear two oscillatory solutions, but in this case the A0-solution is always stable, and the mixed parity solution bifurcates from it.

For a dynamo with magnetic buoyancy the results are different, and we were not able to follow the solutions to as high dynamo numbers as for α-quenching. For positive C_α the steady S0-solution persists over the whole interval that we covered, and it is the only stable solution. That is, we do not find any gap when we replace α-quenching by magnetic buoyancy. For $C_\alpha < 0$ there are oscillatory S0- and A0-solutions, both of which are stable and have similar field geometries.

Acknowledgements. We are grateful to Dainis Dravins, Jianke Li, David Moss, and Günther Rüdiger for discussions and comments on the paper. Most of the computations presented in this paper has been carried out on the Cray X-MP 4/16 (upgraded to Cray Y-MP 4/64 during the course of this work) of the National Supercomputer Centre, Linköping, Sweden. UT would like to thank the High Altitude Observatory, where part of this work was carried out, for hospitality, and the Royal Physiographical Society in Lund for a travel grant.

References

Brooke, J. M., Moss, D., 1994, MNRAS, 266, 733
Bruch, A., Duschl, W. J., 1993, A&A, 275, 219
Cattaneo, F., Hughes, D. H., 1988, J. Fluid Mech., 196, 323
Eardley, D. M., Lightman, A. P., 1975, ApJ, 200, 187
Foglizzo, T., Tagger, M., 1994, A&A, (in press)
Hartmann, L. W., Noyes, R. W., 1987, ARA&A, 25, 271

Horne, K., Saar, S. H., 1991, ApJ, 374, L55
Krause, F., 1967, Habilitationsschrift, University of Jena
Krause, F., Meinel, R., 1988, Geophys. Astrophys. Fluid Dyn., 43, 95
Marsh, T. R., 1987, MNRAS, 228, 779
Marsh. T. R., Horne, K., Shipman, H. L., 1987, MNRAS, 225, 551
Meyer, F., Meyer-Hofmeister, E., 1982, A&A, 106, 34
Milsom, J. A., Chen, X., Taam, R. E., 1994, ApJ, 421, 668
Noyes, R. W., Hartmann, L., Baliunas, S. L., Duncan, D. K., Vaughan, A. H., 1984, ApJ, 279, 763
Rüdiger, G. & Kitchatinov, L. L., 1993, A&A, 269, 581
Rüdiger, G. & Brandenburg, A., 1994, A&A, (submitted)
Rüdiger, G., Elstner, D. & Stepinski, T. F., 1994, A&A (submitted)
Shakura, N. I., Sunyaev, R. A., 1973, A&A, 24, 337
Skumanich, A., 1972, ApJ, 171, 565
Stenflo, J. O., 1989, A&AR, 1, 3
Stepinski, T. F., Levy, E. H., 1988, ApJ, 331, 416
Stepinski, T. F., Levy, E. H., 1991, ApJ, 379, 343
Stix, M., 1972, A&A, 20, 9
Torkelsson, U., Brandenburg, A., 1994a, A&A, 283, 677, Paper I
Torkelsson, U., Brandenburg, A., 1994b, Chaos, Solitons & Fractals, accepted, Paper II
Vishniac, E. T., Diamond, P., 1989, ApJ, 347, 435
Wang, J, C. L., Sulkanen, M. E., Lovelace, R. V. E., 1992, ApJ, 390, 46

This article was processed by the author using Springer-Verlag LaTeX A&A style file version 3.